A R C H I V E S O F M E T A L L U R G Y A N D M A T E R I A L S
Volume 50 2005 Issue 1

R.A. SCHWARZER*

ADVANCES IN THE ANALYSIS OF TEXTURE AND MICROSTRUCTURE[1)]

POSTĘP W ANALIZIE TEKSTURY I MIKROSTRUKTURY

The past decade has seen some remarkable progress in texture analysis. There is no universal method, and the choice depends on the sampled grain structure as well as on the degree of required information. The standard technique for the analysis of *global texture* is X-ray pole figure measurement and ODF calculation. A significant improvement in speed and accuracy has been achieved by using a two-dimensional area detector. An extension to local texture measurement has been made by developing an X-ray scanning instrument. X-ray diffraction is a gentle method which is well suited for conductive, recrystallized and flat bulk as well as delicate, non-conductive, deformed, and fine-grain specimens. *Local texture* of extremely deformed or fine-grain materials can be studied by SAD and RHEED pole-figure measurement in the TEM. Texture analysis on a *grain-specific scale* is performed by automated Kikuchi diffraction (ACOM) in the SEM ("Automated EBSD") and TEM. TEM investigations are indispensable when microstructural features have to be quantified such as Burgers vectors and deformation systems.

Keywords: crystal texture; Kikuchi patterns; BKD; EBSD; SAD; Pole-figure measurement; XRD; Energy dispersive XRD

W minionej dekadzie nastąpił zdecydowany postęp w analizie tekstury, ale jak dotąd brakuje uniwersalnej metody. Wybór metody badawczej zależy od struktury ziaren próbki oraz od rodzaju oczekiwanych informacji.

Standardową techniką analizy *tekstury globalnej* jest pomiar figur biegunowych techniką dyfrakcji rentgenowskiej oraz obliczenia FRO. Znaczną poprawę szybkości i dokładności analizy osiągnięto poprzez zastosowanie 2-wymiarowego detektora powierzchniowego. Rozszerzenie metody o pomiar *tekstury lokalnej* uzskano poprzez rozwój skanującej aparatury rentgenowskiej. Dyfrakcja rentgenowska jest nieniszczącą metodą, która jest stosunkowo łatwa do zastosowania w przypadku płaskich próbek zrekrystalizowanych, nieprzewodzących elektryczności, odkształconych oraz drobnoziarnistych.

Tekstura lokalna materiału silnie odkształconego lub drobnoziarnistego może być badana poprzez pomiary figur biegunowych SAD oraz RHEED w TEM. Analiza tekstury w

* INSTITUT FÜR PHYSIK, TU CLAUSTHAL, D-38678 CLAUSTHAL-Z., GERMANY

[1)] invited lecture

skali poszczególnych ziaren jest przeprowadzana poprzez zautomatyzowany pomiar dyfrakcji Kikuchi (ACOM) w SEM (zautomatyzowany EBSD) i TEM. Badania TEM są niezastąpione wtedy, gdy mikrostruktura musi być scharakteryzowana takimi wielkościami jak wektor Burgersa czy systemy deformacji.

1. Introduction

Natural as well as man-made materials (e.g. minerals, rocks, bones; metals, ceramics, crystalline polymers) are often assumed to behave uniformly with equal strength in all directions, although most of them have a polycrystalline structure. The anisotropy of the individual crystals, however, is only balanced out in case of a large number of grains *and* a random distribution of the grain orientations. In reality, a residual anisotropy is found which varies, depending on the actual statistical distribution of grain orientations — the "crystal texture", "preferred crystal lattice orientations" —, between the extreme values of the anisotropic physical property of interest with which a single crystal of the same material will respond to directional tests. *Local* variations in *crystal texture* as well as the arrangement and type of *grain/phase boundaries* may give rise to *inhomogeneous material properties* which may finally limit the performance of a workpiece. Texture also bears information about the history of materials' processing and use. Therefore, the knowledge of texture is of great concern for quality control in a wide range of industrial applications and for basic materials research.

2. Global texture measurement by X-ray pole figure measurement

The standard techniques of quantitative texture analysis [1, 2 and references therein] are based on X-ray, synchrotron, neutron and electron diffraction. Noticeable advances have been made during the last years by the development of automated X-ray texture goniometers including position sensitive, two-dimensional, CCD, and energy dispersive detectors, and by the introduction of new X-ray optics.

In particular the replacement of the conventional proportional counter by a two-dimensional area detector for acquiring pole-figure data [3] has been a great stride ahead. The two-dimensional diffraction pattern covers a wide section of reciprocal space and is recorded in digital form ("electron film"). The advantages for pole figure measurement are

- increased angular resolution in 2ϑ ($\approx 0.1°$).
- increased resolution in the pole figure angles ($\alpha\beta$) with $\Delta\alpha$ and $\Delta\beta$ ($\approx 0.1°$).
- deconvolution of complex diffraction spectra with overlapping peaks by peak profile analysis.
- peak profile analysis which provides the necessary peak profile parameters for
  - — integral peak intensity → crystal texture.
  - — peak shift → residual stress of the 1st kind.
  - — peak broadening → residual stress of the 2nd and 3rd kind, grain and domain size.

- improved speed. Several X-ray pole figures can be acquired in less than 30 min.
- A sample stage with constant χ tilt and rotation of the sample about its surface normal direction is sufficient rather than a full-range Euler cradle which is required with a conventional proportional counter or with a position sensitive detector.

Since the sample needs only be rotated about its surface normal and can be maintained at a constant χ tilt, the penetration depth of the primary beam is the same for all pole figures and for all pole figure points of one acquisition set-up which results in an improved self-consistence of the experimental X-ray pole figure data. In order to increase sensitivity for the study of thin layers on a flat sample surface, a low angle of incidence is used. In this case, the paths of the secondary beams — which leave the sample at large angles — are short as compared to the path of the primary beam in the sample. Consequently, not only the penetration depth but also the depths of information, i.e. the depths of the probed volumes beneath the surface, are almost constant for all pole figure points and every pole figure [4]. By comparing the results from measurements at different angles of incidence, *texture profiles* and *texture gradients* can conveniently be investigated in-depth beneath the surface with an area detector.

In reflection mode, the pole figures are incomplete with a non-measured area at the outer margin. They may also contain a non-measured central area when acquired at a fixed sample tilt χ with an area detector. It is worth noting that the ODF program has then to accommodate for different non-measured areas in the experimental pole figures [5]. Otherwise the sample has to be set to complementing 2ϑ or χ angles, and additional measurements have to be carried out to fill the "holes" in the pole figures [4], on the expense of longer time for the experiment.

In addition to the symmetry of the crystal lattice, the texture of the sample can posses a symmetry, but in the statistical sense (*sample symmetry*) [6]. As a result of the symmetry of the rolling process, for example, individual orientations in the mid plane of a sheet metal may occur with equal statistical frequency about the rolling, the transverse and the sheet planes (so-called orthorhombic sample symmetry characterized by three mirror planes), but each grain need not (and indeed will not) have its precise symmetrical counterpart. Since the symmetry elements of the sample are referred to the collective of grains rather than the individual crystallites, they lead, in general to non-equivalent crystallographic orientations. Therefore, the statistical sample symmetry has to be strictly distinguished from the crystal symmetry. It is important to mention here that in most of the studies of rolling textures available in literature, the samples have been tacitly assumed to have orthorhombic symmetry without a further check, and characteristic features of texture have been concealed from view by symmetrization. Examples to illustrate the adverse effect of symmetrization are the lost recognition of asymmetric tilt of the c-axes to RD in the rolling texture of pure magnesium (Fig 1) [7]. Similarly, improper orthorhombic symmetrization of the wear texture of copper (Fig. 2) [8], for instance, would obscure the well-developed monoclinic sample symmetry, i.e. the fact that only one mirror plane is present along the directions of shear and sample normal. Correct symmetrization is therefore important to recognize the shear components in the surface texture of rolled sheet metals.

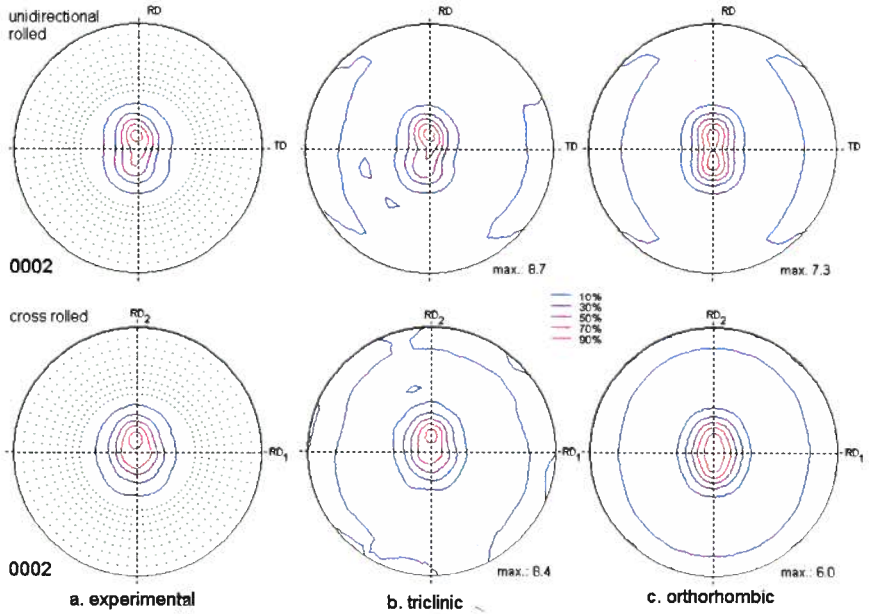

Fig. 1. Texture of pure magnesium after unidirectional hot rolling at 200 °C to 73% reduction in thickness (top) and multi-step cross hot rolling at 350 °C to 85% reduction in thickness (bottom)
a. Experimental 0002 pole figures, b. 0002 pole figures recalculated from ODF under the assumption of triclinic sample symmetry, c. 0002 pole figures recalculated from ODF under the assumption of orthorhombic sample symmetry $l_{max} = 22, \Phi_0 = 5°$

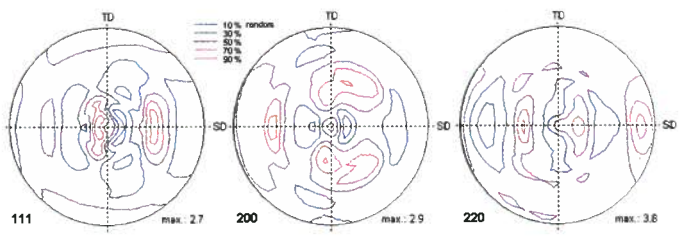

Fig. 2. The texture of copper after a dry-running pin-on-disk frictional wear test. The pole figures have been measured at 15° angle of incidence of the primary X-ray beam with an area detector and recalculated from ODF under the assumption of triclinic sample symmetry ($l_{max} = 22, \Phi_0 = 5°$). SD stands for the direction of shear, TD for the transverse direction in the shear plane

3. An X-ray scanning instrument for texture mapping

Spatial resolution of conventional X-ray pole-figure measurement is often not sufficient to resolve texture gradients in the surface or to study local texture. To tackle these tasks, an X- ray Scanning Instrument (XSI) has been developed for "imaging" the spatial distributions of crystal texture, residual lattice strain, and element composition in

bulk specimens as well as for pole-figure measurement on selected small areas [9-11]. The system is based on a commercial two-circle goniometer and an open Euler cradle (PHILIPS X'Pert MRD goniometer). An X-ray tube with an anode of heavy metal (Mo, W) produces an intense continuous radiation. The primary beam is confined to a small spot by using a diaphragm collimator.

A standard energy dispersive (ED) detector is used for X-ray detection to enable the fast acquisition of a spectrum of several diffraction or fluorescence peaks at a time as well as the deconvolution of overlapping peaks and peak profile analysis for residual lattice strain measurement. The advantages of an ED detector over a position sensitive detector are for texture mapping:

- A high efficiency is obtained since non-filtered ("white") primary beam radiation is used and almost 100% of the intensity falling on the detector is acquired.
- A very high and linear count rate is achieved.
- All diffraction peaks are related to the *same direction* in the specimen-fixed coordinate system, i.e. they represent the same point (α,β) on the pole spheres.
- X-ray fluorescence peaks may be evaluated for element analysis, in addition to diffraction peaks.

Mapping is performed by translating the specimen with a stepping-motor driven x-y stage step by step across a field up to 100 mm by 100 mm wide in a user defined mesh grid. Several distribution maps are constructed on-line at the same time by assigning colors to the pixels which are characteristic for the intensities of diffraction peaks (texture), shift or width of diffraction peaks (residual lattice strain), and the intensities of characteristic fluorescence peaks (element concentrations) in the spectra at the corresponding x-y positions. The sensitivity and resolution of residual strain measurement are limited by the spectral resolution of the solid-state spectrometer system. Also peak broadening due to the finite primary beam and detector apertures have to be considered. With a standard Si(Li) detector lattice strains down to $\Delta a/a = 4 \cdot 10^{-4}$ have been resolved [12]. Pole figures are measured by tilting and rotating the specimen in the Euler cradle through an equal step, equal area, thinned or user-defined angular grid (α,β) on the pole sphere. Spatial resolution is primarily dependent on the size of the X-ray spot and its elliptical elongation by projection on the tilted surface. A practical limit is presently at 0.1 mm for pole-figure measurement and lattice strain mapping, and 0.05 mm for texture and micro X-ray fluorescence element mapping, because of the low intensity of the collimated primary beam.

X-ray mapping is a very gentle method since the specimen is only exposed to X-rays and stays in the atmospheric environment. Measurement is not affected by the degree of plastic deformation. Bulks can be studied irrespective of their conductivity. Due to the large depth of focus with a collimated primary beam, rough surfaces can be imaged. Sample preparation is simple. In most cases the same or similar methods are appropriate as for reflected light microscopy.

Plastic deformation may cause a distinct change of texture in the material which depends on the grain orientations, the mode, degree and rate of deformation. By impressing the jaws of a mechanical testing machine into the coarse-grain surface of a

recrystallized aluminum sheet metal, a rhombic relief pattern has been formed. The sample was then mechanically grinded and polished to a flat mirror such that the pattern was no longer visible. In the texture maps (Fig. 3), however, high pole densities can be seen in regions where the corrugating teeth of the jaws caused a high local deformation, whereas deformation in the grooves of the jaws was low enough to preserve the original texture of the metal sheet [9]. The texture maps of Fig. 3 were acquired simultaneously from the same sample area by measuring the intensities of the 200, 220, 311 overlaid with 222, and 331, peaks at *symmetrical diffraction setting* ($\vartheta_1 = \vartheta_2$). Hence the spatial distributions of pole densities in *sheet normal direction* are shown. The sheet texture did not contribute to these selected diffraction peaks. If some other texture component of the metal sheet is of interest, the specimen has to be tilted away from the symmetrical geometry to an appropriate pole-figure point into which the sheet is diffracting.

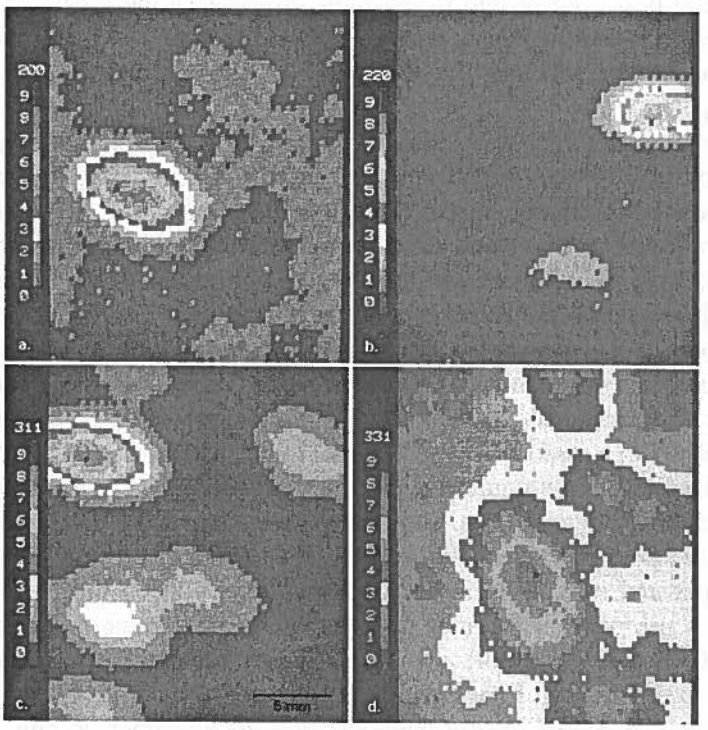

Fig. 3. Texture maps of a compression pattern in aluminum revealing local plastic deformation. (a) {200} reflections b) {220} reflections c) {311} and {222} reflections d) {331} reflections

4. Local texture measurement by electron diffraction

As a supplement to the established techniques of global texture measurement by X-ray, synchrotron radiation and neutron diffraction, electron diffraction techniques on

computer-controlled SEM and TEM have been developed for the study of preferred crystal lattice orientations on a grain-specific scale [2]. Depending on the problem to be solved, a "statistical texture" and an "individual grain orientation" approach have been made:

- Pole figures of small areas are obtained from thin foils in SAD or from bulk surfaces in RHEED mode of the TEM.
- *A*utomated *C*rystal *O*rientation *M*easurement / *M*apping (*ACOM*) grain by grain by interpreting Kikuchi patterns in the SEM or TEM is about to become the working horse of modern microstructure analysis.

4.1. On-line measurement of pole figures with the TEM

*S*elected *A*rea electron *D*iffraction (SAD) in the TEM is the conventional technique to study the crystal structure of thin films at a high spatial resolution. The distributions of intensity along the diffraction rings are a quantitative measure of the volume fraction of grains with preferred orientations related to the particular diffraction vectors ("pole densities"). SAD pole figures [13 - 15] are acquired on-line by measuring the variations of diffracted intensities along selected diffraction rings at consecutive specimen tilts either by deflecting, under computer control along a cone of semi-apex angle $2 \cdot \vartheta$ the diffraction patterns behind the objective lens or the primary beam before the specimen [14]. The diffracted intensities are recorded either in diffraction mode with a Faraday cup (Fig. 4a), or in imaging mode by taking the current from the dark field images (Fig. 4b). Speed and accuracy have been improved significantly with a high-resolution CCD camera used as an area detector by grabbing the whole diffraction patterns [16]. In this case, no beam deflection is required and the specimen is only tilted about the axis of the side-entry goniometer stage. A future extension to high speed ACOM will be the extraction of spatial *and* orientation parameters from digitized consecutive dark-field images for selected hkl reflections and for a range of sample tilts.

Textures of thin surface films on bulk substrates are measured in the TEM with a backscattering set-up using a special RHEED specimen holder [17] (Fig. 4c). The specimen is kept at a constant tilt angle close to grazing incidence of the primary beam and rotated under computer control in incremental small steps about its surface normal. The backscatter texture patterns are recorded at each step with a CCD camera. The advantages of RHEED pole figures over grazing incidence X-ray pole figures are an extreme surface sensitivity and a high speed. The results obtained from samples subjected to frictional and to abrasive wear agree well with X-ray pole figures measured with an area detector and a flat angle of incidence [8], although grain statistics in electron diffraction is much lower.

Correction procedures have been developed to interpret quantitatively the SAD and RHEED intensities in terms of pole-to-volume distribution [18]. The orientation distribution function (ODF) is calculated from experimental SAD and RHEED pole figures by applying the iterative serial expansion method similar as in X-ray texture analysis [4]. The different shapes of non-measured areas have to be taken into account.

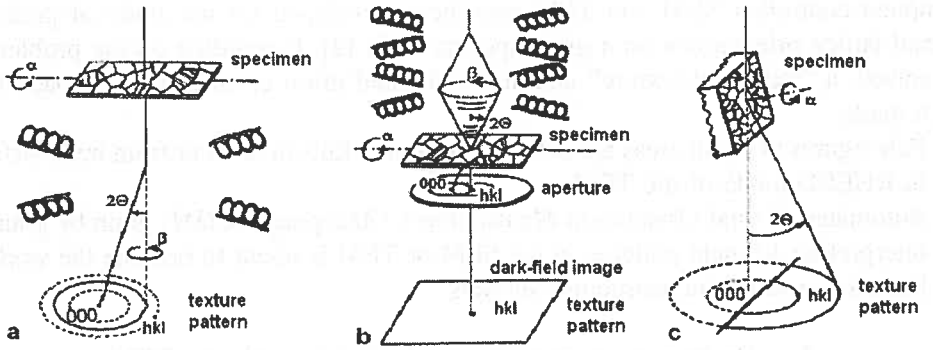

Fig. 4. The acquisition of pole figures in the TEM. a. Circular post-lens deflection. Intensity is measured on-axis with a Faraday cup beneath the phosphor screen. b. Conical pre-lens deflection. Intensity is measured from the dark field image or with a Faraday cup (SAD mode), c. Backscatter set-up. The diffraction patterns are acquired in digital form with a CCD camera

Applications of this technique have been the study of deformation texture of shear bands and deformation bands in cubic and hexagonal materials [19, 20]. Spatial resolution in SAD transmission pole figure measurement is a few microns. The probed area ranges up to about 100 μm diameter in SAD and about 100 μm by 500 μm in RHEED pole figure measurement.

4.2. Individual grain orientation measurement

*A*utomated *C*rystal *O*rientation *M*easurement (*ACOM*) by *B*ackscatter *K*ikuchi *D*iffraction (*BKD*) in the SEM, also named "*Automated EBSD*", has become an invaluable tool of materials science and geology during the last decade [21, 22]. The broad acceptance of Automated EBSD is based on the availability of crystallography in the SEM in a much easier and efficient way than was previously possible by the acquisition of electron spot and channeling patterns in transmission or reflection diffraction. ACOM is performed in the SEM by digitally scanning the beam spot across the specimen, acquiring and transferring one backscatter Kikuchi pattern after the other to the computer, indexing it and calculating the crystal orientation of the grain under the beam spot. Speed is between 30.000 and 200.000 orientations per hour, depending on the hardware. If intragranular structure is of no concern, it is sufficient to acquire the orientation of each grain only once, and iterative mesh refinement [23] has proven very effective by concentrating measurement along grain boundaries. Mesh refinement is inadequate if the microstructure contains twinned grains or if a broad grain size distribution is present.

High energy electrons are strongly forward scattered when impinging on a bulk surface. Therefore, the specimen surface has to be steeply inclined in the SEM at typically 20° to 30° to the beam, in order to produce a backscatter Kikuchi pattern of

sufficient intensity. This high specimen tilt has several unfavorable consequences on digital beam scanning:

1. The diffraction geometry, in particular the position of the pattern center (which marks one of the reference directions of the orientation frame) and the distance from beam spot to screen ("camera length"), changes from one scanning step to the next.
2. The beam spot runs out of focus when scanning down the specimen line after line.
3. Short working distances on which the microscope lenses have been optimized for obtaining a high resolution and high beam current cannot be used, if large specimens have to be accommodated.
4. The beam spot on the specimen as well as the crystal orientation maps and conventional SEM images, when taken at the same steep specimen tilt, are heavily foreshortened.
5. Standard secondary electron and backscatter electron detectors produce uneven "illumination" of the images since the signal height is modulated as a function of the distance between the detector and the beam spot.
6. A steep specimen tilt is incompatible with most quantitative EDS programs which is an obstacle to simultaneous element analysis and crystal orientation measurement.

The software of an advanced EBSD system must account for the first difficulties. In addition to driving the digital beam scan, it has to perform, at all magnifications and working distances, the automated "on-the-fly" calibration of both the position of the pattern center and the beam spot-to-screen distance, as well as dynamic focusing of the probe-forming lens as a function of the beam spot position [21]. Otherwise errors in calculated grain orientations may exceed several degrees or indexing may fail, in particular at low magnifications. For that purpose, the SEM has to be operated under full ACOM software control which comprises the setting of the final-lens current, control of camera operation and synchronization of pattern acquisition, reading the actual microscope magnification and accelerating voltage, and — unless the pattern background is not modeled — control of the digital signal processor and modes of SEM operation to switch between imaging and spot mode for the automated acquisition of flat images. A simple test on the accuracy of automated system calibration can be made by measuring across a large field on a single crystal and checking the uniformity of orientation data.

The geometry of a Kikuchi pattern is unique for the crystal structure and the crystal lattice orientation of the grain under the beam. It is sufficient for indexing to know the *positions and widths* of some bands in the pattern. The geometrical features of a pattern are extracted after Radon transformation by automated pattern recognition. Details of the indexing routine can be found in [24]. The crispness of the pattern, called "*P*attern *Q*uality" (PQ), is an indication of the perfection of the diffracting crystal volume. Pattern Quality is obtained straightforward from the magnitudes of high Fourier frequencies of a 1D FFT in band normal direction across the centers of the Radon peaks [25]. The calculated values of Pattern Quality are not much affected by pixel noise, because the Radon transformation of the Kikuchi pattern corresponds to

an integration of band edge intensities along the particular band, and hence noise along this direction is fairly well averaged off. In addition, the 1D Fourier coefficients describe the averaged shape of every evaluated band edge only in the direction *perpendicular* to the particular band rather than over *all polar* directions in the diffraction pattern. Pattern Quality can be used to discriminate between deformed and recovered or recrystallized grains in a microstructure. Pattern quality maps of coarse grain metals clearly display grain boundaries and surface scratches, and often show features which look like a dislocation network. A diffuse pattern, however, may also result from a foreign surface layer such as carbon of excessive thickness (which may have been deposited by intention to avoid specimen charging), a contamination layer due to poor vacuum conditions, a deformation layer from inadequate sample preparation, or an insufficiently focused beam spot.

A similar computer program as for BKD in the SEM [21] including digital beam scan has been implemented on a PHILIPS EM 430 TEM [26]. In addition to grain orientations, structural features such as dislocation line directions or grain boundary normals can be indexed. In particular Burgers vector analysis and the determination of deformation systems is conveniently performed with the aid of the computer program [24, 27]. Specimen tilt about two axes is simulated on spot and Kikuchi patterns to check suitable reflections for fulfillment of the $\mathbf{g} \cdot \mathbf{b} = 0$ criterion. Allowance is made for image rotation as a function of accelerating voltage, magnification and diffraction length. The simulated angular settings are then transferred from the computer to the double tilt specimen holder under visual control of the image whereby unwanted specimen drifts, as a consequence of extended tilt movements, can easily be corrected.

Transmission Kikuchi patterns in *M*icro*B*eam electron *D*iffraction (MBD) enable more reliable orientation measurements than spot patterns in the TEM do. Film thickness may range from the mean free path length of the primary beam electrons to some micrometers, depending on the accelerating voltage and the density of the particular material. The possibility to use thick specimens in the TEM is a major advantage of Kikuchi diffraction. Thin foils, suitable for spot or CBED patterns, are often difficult to prepare and may hardly be representative for the bulk material. In addition, local foil bending is reduced significantly with increasing thickness and will so less affect accuracy of measured orientation data. The adverse effect of wrinkled thin foils becomes apparent by the formation of bent contours in crystal orientation maps.

The beam convergence is not relevant for the formation of a Kikuchi pattern, as inelastic scattering will spread out the primary beam into all directions, that is over a much larger angular range than can ever be obtained by means of focusing an electron lens on the specimen at a short distance. Hence, the term CBED is not appropriate for Kikuchi diffraction with regard to local orientation measurement, although Kikuchi lines are also present in CBED patterns. They are sometimes used as an alternative technique for obtaining a high spatial resolution with older TEM. CBED suffers from the excessive widening of the diffraction spots due to the increasing primary beam aperture when the beam is focused on the grain of interest. The patterns are therefore of very limited use for crystal lattice orientation measurement. CBED patterns are

used on a grain-specific level either for the determination of local foil thickness and structure potentials of the crystal lattice, or for the determination of crystal lattice symmetry (space and point group), for phase identification, for the characterization of stacking faults and Burgers vectors, and for residual strain measurement.

The grain orientations are commonly depicted in pseudo-colors on the scanning grid to form *C*rystal *O*rientation *M*aps (*COM*) [28] which represent "images" of the microstructure with the advantage of providing quantitative orientation contrast. In a similar way, misorientations across grain boundaries, Σ values of grain boundaries, or other microstructural characteristics and derived entities are visualized by staining the grains in the micrograph with specific colors. All grain boundaries exceeding some tenth of a degree are identified. Stereological as well as orientation data, as sensitive indicators of the production process, are readily available. ACOM thus enables a major progress in the quantitative characterization of microstructure.

The principal objectives of ACOM in the SEM are a quantitative description of the microstructure of selected areas on *bulk surfaces* in a short time on a grain-specific level by the determination of quantitative, statistically significant data sets of crystal orientations, misorientations, the CSL character of grain boundaries (Σ), local crystal texture (pole figures, ODF, MODF, OCF) and derived entities, and phase discrimination [29] when possible phases in a sample are supposed to be present. As a further characteristics, the *crystallographic direction* of the grain boundary normal n can be determined by measuring the spatial inclination of the grain boundary plane, e.g. by serial sectioning. The correlation of spatial and orientation parameters and the high speed of ACOM with the SEM will thus facilitate a 3D reconstruction of the microstructure of the bulk by merging the two conventional but still separated branches of microstructure characterization that are quantitative stereology and texture analysis to a more general concept of (3D) orientation stereology [30].

In practical work, spatial resolution is limited to about 50 nm with backscatter Kikuchi patterns in the SEM by the volume of the interaction sphere of backscattered primary electrons with the specimen, and to about 10 nm with transmission Kikuchi patterns in the TEM. It is worth noting that the high spatial resolution of the TEM can only be utilized with columnar grains of this diameter and an elongation of some hundred nanometers or more in beam direction. If the crystal is much thinner, spot patterns are formed rather than Kikuchi patterns. Some alleviation with thin foils can be obtained by increasing inelastic scattering of the primary beam when entering the specimen. This can be achieved by either reducing the accelerating voltage and/or by placing the thin sample foil bottom down on an amorphous support film. The crystalline sample foil should not be thicker than the average grain size, otherwise the diffraction patterns of piled up grains will overlap and (automated) pattern indexing will fail.

If neighboring grains are studied, orientation differences can be measured automatically down to 0.1° with transmission and < 0.5° with backscatter Kikuchi patterns. When evaluating the crystal lattice orientations with respect to the workpiece, additional errors may be introduced by misalignments of the sample and the microscope. An outstanding feature of electron microscopy is the ability to produce a high-resolution image

and alternatively a diffraction pattern of the same selected area by simply switching from imaging to diffraction mode of operation.

4.3. Example of application of ACOM with the SEM

Continuous thin metal layers deposited on a solid substrate by sputtering or evaporation under high vacuum or by electroplating often exhibit a marked fiber texture. Grain structure is increasingly becoming important when the dimensions of the layers are in the range of average grain size. This is in particular the case with interconnect lines in modern microelectronic circuits. Copper, due to its high electromigration resistance, is one promising candidate to replace aluminum as the standard metallization material. Polycrystalline copper, unlike silicon single crystals, cannot be etched to sharp contours. Therefore copper layers are usually electroplated into narrow "damascene" trenches in the substrate to achieve extremely narrow lines with sharp edges. Thus, they are subjected to geometric constraints on grain growth by the trench sidewalls and the bottom during deposition and recrystallization.

In this example [31], about 1 μm thick copper layers have been electroplated into trench-structured SiO_2/Si substrates. The trenches were 1.0 μm wide, 0.5 μm deep and PVD coated with 50 nm tantalum as a barrier layer. In addition, a PVD copper seed layer has been deposited at 50°C. After the electroplating process, the wafers were annealed for 10 min. at 120°C. Finally the continuous copper layer has been removed by chemical-mechanical polishing (CMP) down to the damascene trenches.

Fig. 5. Competing grain growth during electroplating copper interconnect lines into damascene trenches may result in the formation of a central seam. The crystal orientation map shows grains grown from the bottom and grains grown from the sidewalls of the trenches

In the crystal orientation maps (Fig. 5), the crystal orientations are represented by pseudo-colors (or here in gray tone) in every pixel element. All grains are clearly discriminated from each other, in contrast to conventional SEM images. A central seam of grain boundaries has been formed in several interconnect lines. The ODF and pole figures have been calculated with the series expansion method [5] from the measured crystal orientations, separately for those grains which fill an interconnect line at full width ("bamboo grains") and for those grains which form the central seam. Preferred $<111>$ and $<115>$ orientations have been found for both types of grain. However, the fiber axes have been aligned perpendicular to the specimen normal direction for the

bamboo grains, but perpendicular to the trench walls for the grains forming the central seam. <115> is the twin orientation to <111> which is the direction of fastest grain growth in copper. The conclusion is drawn that competing grain growth had occured from the bottoms and from the side walls of the trenches.

REFERENCES

[1] H.J. Bunge, C. Esling, Texture et Anisotropie des Matériaux, Techniques de L'Ingenieur, Traité Matériaux Métalliques M 605, 1-39, Paris 1998.
[2] R.A. Schwarzer, Materials Science Forum, **287-288**, 23-60 (1998).
[3] H. Bunge, H. Klein, Z. Metallkunde **87**, 465-475 (1996).
[4] B. Schäfer, Materials Science Forum **273-275**, 113-118 (1998).
[5] K. Helming, U. Preckwinkel, Solid State Phenomena **105**, 71-76 (2005).
[6] H.-J. Bunge, Texture Analysis in Materials Science — Mathematical Methods. Butterworths, London 1982 (Reprint: Cuvillier Verlag, Göttingen 1993)
[7] A.K. Singh, R.A. Schwarzer, Z. Metallkunde submitted for publication.
[8] R.A. Schwarzer, Solid State Phenomena **105**, 195-200 (2005).
[9] R.A. Schwarzer, Steel Research **64**, 570-574 (1993).
[10] R.A. Schwarzer, M. Wehrhahn, Proc. 11th Intern. Conf. Textures and Microstructures, Xi'an (China) 176-181 (1996).
[11] A.H. Fischer, R.A. Schwarzer, Materials Science Forum **273- 275**, 255-262 (1998).
[12] A.H. Fischer, R.A. Schwarzer, Materials Science Forum **273-275**, 673-677 (1998).
[13] F.J. Humphreys, Textures and Microstructures **6**, 45-62 (1983).
[14] R. Schwarzer, Beitr. elektronenmikroskop. Direktabb. Oberfl. (BEDO) **18**, 61-68 (1985).
[15] H. Weiland, S. Panchanadeeswaran, Textures and Microstructures **20**, 67-86 (1993).
[16] R.A. Schwarzer, N.C. Krieger Lassen, B. Schäfer, Proc. 11th Intern. Conf. Textures of Materials (ICOTOM-11), Xi'an (China) 170-175 (1996).
[17] B. Schäfer, R.A. Schwarzer, Materials Science Forum **273- 275**, 223-228 (1998).
[18] R. Schwarzer, BEDO **16**, 131-134 (1983).
[19] R.A. Schwarzer, Proc. EUREM 88, York 1988, Inst. Phys. Conf. Ser. No. **93/2**, 23-24 (1988).
[20] A. Huot, R.A. Schwarzer, J.H. Driver, Materials Science Forum **273-275**, 319-326 (1998).
[21] R.A. Schwarzer, Micron **28**, 249-265 (1997).
[22] R.A. Schwarzer, The Physics of Metals and Metallography **96**, Suppl. 1, 104-115 (2003).
[23] R.A. Schwarzer, Microscopy and Microanalysis **5**, Suppl. 2, 242-243 (1999).
[24] S. Zaefferer, R.A. Schwarzer, Z. Metallkunde **85**, 585-591 (1994).
[25] R.A. Schwarzer, J. Sukkau, Adv. Engin. Materials **5**, 601-606 (2003).
[26] R.A. Schwarzer, J. Sukkau, Materials Science Forum **273-275**, 215-222 (1998).

[27] S. Zaefferer, Adv. Imaging and Electron Physics **125**, 355-414 (2002).
[28] D. Gerth, R.A. Schwarzer, Textures and Microstructures **21**, 177- 193 (1993).
[29] R.A. Schwarzer, Analytical and Bioanalytical Chemistry (ABC) **374**, 699-702 (2002).
[30] H.J. Bunge, R.A. Schwarzer, Adv. Engin. Materials **3**, 25-39 (2001).
[31] A. Huot, A.H. Fischer, A. von Glasow, R.A. Schwarzer, Proc. 5th Intern. Workshop on Stress-Induced Phenomena in Metallization, AIP Conference Proceeding **491**, 261-264 (1999).

Received: 24 January 2005.